Light-scattering studies of soft external lattice modes in metallic Na_xWO_3

E. J. Flynn*
The James Franck Institute and The Department of Physics, The University of Chicago, Chicago, Illinois 60637
(Received 4 October 1978; revised manuscript received 30 May 1979)

Soft vibrational excitations associated with successive structural phase transitions in metallic Na_xWO_3 with $0.5 < x < 1$ have been studied over the temperature range $3 < T < 500$ K. The Raman spectra were recorded in the low-frequency region $150 \gtrsim \omega \gtrsim 10$ cm^{-1} using an iodine filter for the attenuation of parasitically scattered light. Transition temperatures determined in the Raman measurements agree quantitatively with the results of other investigations in which the phase transitions in Na_xWO_3 were also detected, especially the x-ray work of Clarke who proposed a unique sequence of octahedral tilt structures for the four distinct phases in Na_xWO_3. A comparison of the group-theoretical selection rules for Raman scattering with the temperature-dependent light-scattering data serves not only to confirm the space-group assignments due to Clarke, but also provides evidence of the rigidity of the WO_6 units, a physical property that dominates the thermodynamic, structural, and vibrational properties of Na_xWO_3.

I. INTRODUCTION

The sodium-tungsten bronzes constitute one member of a class of solid solutions M_xWO_3 in which the solute ions M (usually alkali metal) occupy "voids" or "tunnels" within a network of corner-linked WO_6 octahedra.[1,2] Most remarkable is the ability of the tungsten-oxide host to crystallize in various lattice configurations (cubic, tetragonal I, tetragonal II, hexagonal, etc.), depending on the concentration x and the size of the interstitial ions. Some of the known alkali-tungsten bronzes are given in Table I.

The concentration-dependent electrical, optical, and structural properties of the tungsten bronzes have stimulated considerable research effort, especially in the case of Na_xWO_3, which can be prepared over almost the entire concentration range $0 < x < 1$.[3]

TABLE I. Alkali-tungsten-bronze crystal structure vs concentration.

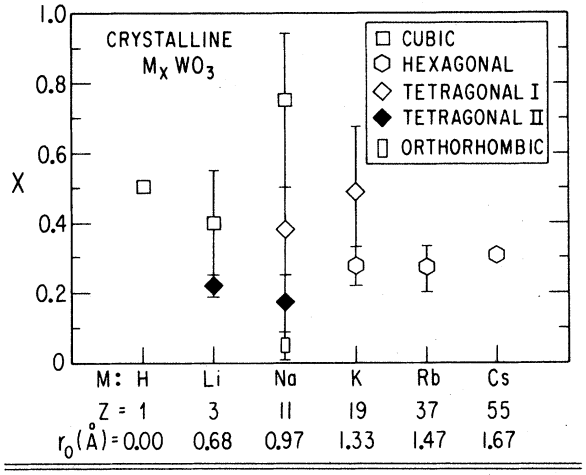

The tetragonal II–tetragonal I phase boundary at $x = 0.22$ is the threshold for metallic conductivity in these materials, while the $x = 0.5$ phase boundary adjoins the tetragonal-I superconductors and the normal metals of the high-concentration regime $0.5 < x < 1$, the so-called "cubic" sodium-tungsten bronzes which have long been known to be closely related in structure to the simple cubic ABO_3 perovskite compounds.[4–8]

This paper is concerned primarily with inelastic light scattering studies of metallic, pseudoperovskite Na_xWO_3. The experimental work described here constitutes the first light scattering investigation of "cubic" Na_xWO_3, among several reported in the literature,[8,9] in which the serious technical difficulties posed by Raman spectroscopy of these metals have been properly and successfully addressed. Furthermore, the microscopic, dynamical information provided by Raman spectroscopy is complementary to the results of transport,[10–13] optical,[6,7] x-ray,[13] neutron,[4] and NMR[14,15] measurements which have been carried out on "cubic" Na_xWO_3 over the past 20 years. In particular, single crystals belonging to this subclass of Na_xWO_3 have been shown, via the temperature dependence and symmetry properties of Raman active soft modes in Na_xWO_3 reported by Flynn, Solin, and Shanks,[16] and the x-ray work of Clarke,[17] to undergo a unique sequence of soft-mode induced displacive structural phase transitions that bears a special, canonical relationship to similar structural sequences exhibited by insulating ABO_3 perovskites in which the atomic displacements correspond to rotations of the BO_6 octahedral units.[18] Usually these octahedral tilt distortions involve a rotation angle ϕ that is small ($\phi \leq 5°$) (Ref. 18): Thus the BO_6 oc-

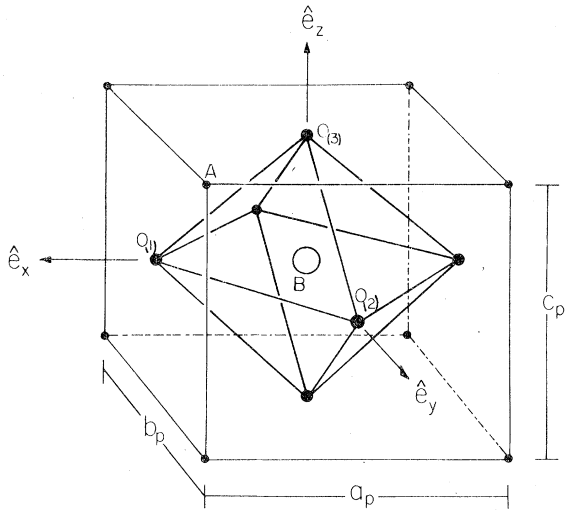

FIG. 1. ABO_3 perovskite primitive cell.

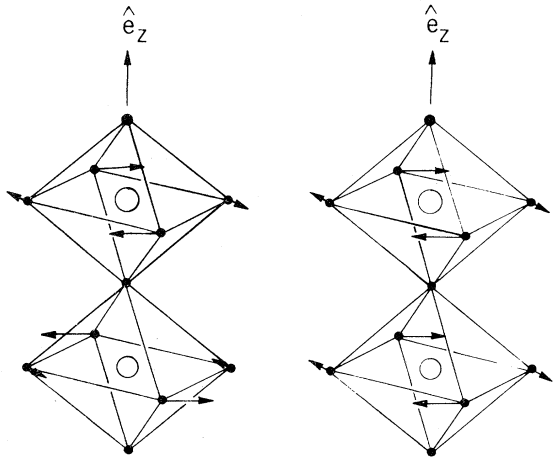

FIG. 2. "Negative" and "positive" tilts about e_z, where corner-linked octahedra along the tilt axis are rotated by the same angle, but in the opposite sense and in the same sense, respectively.

tahedra remain approximately undistorted, or regular, to first order in φ.

Motions of the rigid BO_6 unit, shown in Fig. 1, involve only displacements of the oxygen atoms from equilibrium. Relative to the origin (chosen at atom B) $O_{(1)}$, $O_{(2)}$, and $O_{(3)}$ occupy the positions $\vec{r}_i = \frac{1}{2}\vec{a}_i$, $i = 1,2,3$ where the $\vec{a}_i$ are the primitive translations of the perovskite lattice. Hence, a rotation of the octahedron about e_z will impart to atom $O_{(i)}$ the displacement $\vec{u}_i$,

$$\vec{u}_i = \varphi e_z \times \vec{r}_i \quad . \tag{1}$$

These displacements can be accommodated in the lattice of rigid BO_6 octahedra only by the simultaneous rotation of adjacent octahedra. The rigid tilt configurations most frequently encountered in perovskites are the "positive" and "negative" tilts,[18] illustrated in Fig. 2, where alternate octahedra along the tilt axis are rotated in the same or opposite sense, respectively. Here the displacement $\vec{u}_i(\vec{l})$ of the oxygen atom whose initial position is $\vec{r}_i(\vec{l})$,

$$\vec{r}_i(\vec{l}) = \vec{r}_i + l_1\vec{a}_1 + l_2\vec{a}_2 + l_3\vec{a}_3 \quad , \tag{2}$$

(l_1, l_2, l_3 integers) is given by

$$\vec{u}_i(\vec{l}) = (-1)^{l_1+l_2}\vec{u}_i \quad , \tag{3}$$

for the positive tilt, or by

$$\vec{u}_i(\vec{l}) = (-1)^{l_1+l_2+l_3}\vec{u}_i \quad , \tag{4}$$

for the negative tilt. Any combination of negative and positive tilts about e_x, e_y, and e_z can be imposed simultaneously on the perovskite structure. In the notation of Glazer,[18] each of the 23 distinct rigid tilt structures is denoted by a symbol such as $a^-b^0c^-$. In this example, unequal negative tilts about e_x and e_z, and no tilt about e_y are implied.

The long-range electrostatic interactions which account for the displacive phase transitions exhibited by dozens of ceramic perovskites[19] are screened by the conduction electrons in the case of metallic Na_xWO_3. Consequently, the collective ionic displacements and soft-mode behavior in Na_xWO_3 are somewhat anomalous, inasmuch as the forces to be associated with these phenomena are less evident. Historically, special interest in "cubic" Na_xWO_3 has stemmed from the dubbing of these materials as "ferroelectric metals,"[20] a term coined by Anderson and Blount[20] in proposing a description of the structural phase transitions in the A-15 superconductors V_3Si and Nb_3Sn that occur just above their superconducting transition temperatures. The information conveyed by the term "ferroelectric" in this context is twofold. First, the displacive phase transition exhibited by the "ferroelectric metal" is second order; it follows that the order parameter of the transition is a set of atomic displacements having the symmetry of a Raman active optic lattice vibration in the ordered phase (i.e., below the transition temperature T_0). Second, the ordered phase is structurally equivalent to a ferroelectric: A polar phase for $T < T_0$ results from an optic-phonon instability, or soft mode, in analogy with ferroelectric transitions such as the cubic (O_h^1) to tetragonal (C_{4v}^1) transition in the perovskite $BaTiO_3$.[21] The soft mode in such cases belongs to $\vec{k} = 0$, thereby preserving the number of atoms per unit cell. Soft-mode behavior associated with the cubic to tetragonal transition in Nb_3Sn or V_3Si has never been observed.[19] However Na_xWO_3 has been considered to be a possible "ferroelectric metal" by virtue of its pseudoperovskite structure, closely related to that of

$BaTiO_3$, and the presence of a high-temperature structural phase transition, the existence of which had been established by a number of experimental techniques prior to the recent observation of soft modes in Na_xWO_3 via Raman scattering.[22] The key results from three such experiments are discussed in the following paragraph.

The work of Ingold and DeVries[7] actually provided evidence of two phase transitions in Na_xWO_3 single crystals, from an optically isotropic, cubic structural phase to a tetragonal phase, characterized by optical birefringence, involving a very slight distortion of the cubic structure. Experimentally the cubic and tetragonal phases were distinguished by the appearance in polarized reflectance, within a finite-temperature interval (T_L, T_U), of light and dark "fringes" corresponding to twinned single-crystal tetragonal domains. Adjacent domains were evidently twinned along (110) planes. The optical anisotropy of the crystal surfaces thus observed was contrasted with the uniformly dark field of view, characteristic of the cubic, isotropic phase, obtained by heating the crystals above T_U or cooling below T_L. Furthermore the upper and lower transition temperatures were x dependent. Next, Inaba and Naito[10] reported a concentration-dependent specific-heat anamoly in Na_xWO_3 indicative of a second-order phase transition; the observed transition temperatures were in agreement with the upper transition temperatures $T_U(x)$ given by Ingold and DeVries. Finally, the temperature dependence of the quadrupole coupling constant (QCC) for Na^{23} reported by Bonera *et al.*[14] indicated the vanishing of quadrupole-interaction induced fine structure in magnetic resonance at and above the high-temperature phase transition at $T \approx T_U(x)$. In the case of a "positive" or "negative" octahedral tilt, respectively, the quadrupole moment of the nucleus A in ABO_3 couples to the rotation-angle order parameter linearly (QCC proportional to ϕ) or quadratically (QCC proportional to ϕ^2). Therefore, according to Borsa,[23] the mean-field behavior $\phi \propto (T_U - T)^{1/2}$ can be inferred from the observed temperature dependence of the QCC $[\propto (T_U - T)^{1/2}]$ if one assumes that a single "positive" octahedral tilt is acquired in Na_xWO_3 at a second-order displacive phase transition. The corresponding one-tilt structure is denoted by $a^0a^0c^+$ in the notation of Glazer.

The NQR results for Na_xWO_3 can be compared to similar measurements carried out on $KMnF_3$,[23] for example, in which the second-order cubic $(a^0a^0a^0)$ to tetragonal $(a^0a^0c^-)$ transition at temperature T_0 entails a single "negative" tilt, so that, for K,[39] the QCC is proportional to $(T_0 - T)$.

The above described experimental account of the phase transitions in the supposed "ferroelectric metal" Na_xWO_3, is deficient in several ways. First, the nature of the low-temperature phase transition in Na_xWO_3, characterized by the vanishing of optical birefringence below the temperature $T = T_L$ has not been addressed. Evidently the low-temperature transition, observed in the reflectivity experiment of Ingold and DeVries,[7] has either been ignored or remained undetected in other investigations, including the specific-heat and NQR experiments mentioned above, as well as x-ray and neutron[4] crystallography, and electrical[11] and thermal[12] conductivity measurements which have been reported in the time between the work of Ingold and DeVries and the recent light scattering experiments of Flynn *et al.*,[16] and the x-ray work of Clarke.[17] Second, the twinning of tetragonal domains along (110) planes reported by Ingold and DeVries is *not compatible* with the one-tilt tetragonal structure proposed by Borsa. The cubic $(a^0a^0a^0)$ to tetragonal $(a^0a^0c^+)$ high-temperature transition implied by the NQR data would be characterized by adjoining tetragonal domains corresponding to independent choices of the "positive" tilt axis, i.e., $a^0a^0c^+$, $a^0c^+a^0$, and $c^+a^0a^0$ regions twinned along (100), (010), and (001) domain walls. Finally, these experiments and others addressed to the structural and dynamical properties of "cubic" Na_xWO_3 offer no conclusion regarding the status of sodium-tungsten bronze as a "ferroelectric metal." The NQR results do not constitute a structural determination, while past x-ray and neutron crystallographic work, carried out prior to Clarke's measurements, has been unsuccessful. In addition, Raman spectra of "cubic" Na_xWO_3 reported by Scott *et al.* are spurious.[8] These spectra were attributed by Salje[9] to vibrational features in compounds of sodium and tungsten derived in thermal decomposition of Na_xWO_3.

The Raman scattering experiments of Flynn *et al.*,[16] have shown for the first time the existence of a soft optic mode in metallic Na_xWO_3 associated with a high-temperautre phase transition at $T \approx T_U(x)$, i.e., the transition temperatures reported by Ingold and DeVries. The soft-mode frequency $\omega_u(T)$ approximately obeyed $\omega_u(T) \propto (T_U - T)^{1/2}$. The temperature-dependent Raman data indicated further the presence of two additional low-temperature structural transitions in Na_xWO_3, characterized by the emergence at the transition temperature $T = T_M(x)$ of a second Raman active mode whose temperature-dependent frequency $\omega_l(T)$ exhibited a step-wise discontinuity at the lower transition temperature $T_L(x) < T_M < T_U$.

These Raman scattering results were confirmed by Clarke,[17] who carried out the first definitive x-ray studies on the "cubic" sodium-tungsten bronzes. The transition temperatures T_U, T_M, and T_L occur at phase boundaries that define a structural sequence in Na_xWO_3 with $0.6 \leq x \leq 0.94$. The results of these x-ray measurements, together with the results of the above described reflectivity, specific heat, NQR, and Raman measurements are shown in the phase diagram in Fig. 3. The transition temperatures deter-

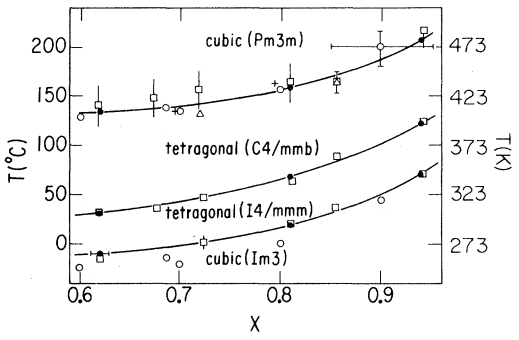

FIG. 3. Phase diagram for Na_xWO_3: □, this work; ●, Clarke (Ref. 17) (x ray); ○, Ingold and DeVries (Ref. 7) (polarized reflectance); Δ, Bonera *et al.* (Ref. 14) (NQR); +, Inaba and Naito (Ref. 10) (specific heat).

mined by different techniques are in good agreement. Note in particular that the tetragonal-tetragonal phase boundary was detected only in the light scattering and x-ray experiments. The analysis of Weissenberg and Debye-Scherrer x-ray photographs by Clarke provided unambiguously (i) the crystal class, (ii) the Bravais lattice type, and (iii) the independent lattice parameters a_p, b_p, and c_p (the three smallest W–W distances), in each of the four phases of Na_xWO_3 with $x \geq 0.6$: simple cubic ($Z_0=1$, $a_p=b_p=c_p$; $T \geq T_U$); simple tetragonal ($Z_0=2$, $a_p=b_p \neq c_p$; $T_M < T < T_U$); body-centered tetragonal ($Z_0=4$, $a_p \neq b_p=c_p$; $T_L < T < T_M$); body-centered cubic ($Z_0=4$, $a_p=b_p=c_p$; $T < T_L$). Here Z_0 is the number of formula units per primitive cell. Clarke proposed that the WO_6 units remain regular or undistorted in spite of the structural phase transformations. This assumption, added to the above crystallographic information, implies for Na_xWO_3 a unique sequence of positive-tilt structures $a^0a^0a^0$, $a^0a^0c^+$, $a^0b^+b^+$, $a^+a^+a^+$ which has not been previously observed in any other perovskitelike compound. Nevertheless this structural sequence has been anticipated theoretically from thermodynamic and group theoretical considerations. In the context of the Landau theory of crystallographic phase transitions,[24–28] the three "positive" tilts in Na_xWO_3 occur sequentially with decreasing temperature via re-orientation of the vector-order parameter whose components are proportional to the amplitudes of the three equivalent lattice distortions which transform as the BZ (Brillouin zone) boundary representation M_3.

Although the octahedral-tilt model of Na_xWO_3 has been convincingly inferred from the x-ray results, it is to be emphasized that direct evidence for the regularity of the WO_6 octahedra—the assumption that is central to this model—is not provided by the x-ray data, inasmuch as the displacements of the oxygen atoms relative to their positions in the perovskite structure could not be measured, due to the weak scattering power of oxygen relative to tungsten. However, the regularity of the octahedra can be correlated with the rigidity of the WO_6 units, a physical property that is clearly manifested in the vibrational spectra recorded in Raman scattering. It will be shown below that the Raman active soft modes, consisting of coupled rigid rotations of the WO_6 octahedra about the orthogonal axes e_x, e_y, and e_z, are intimately related to the sequence of octahedral-tilt structural phases. The link between the structural and dynamical information yielded by x-ray diffraction and by light scattering, respectively, is provided by the Landau theory.

Light scattering from metals and other materials that are opaque to visible light is technically difficult, but growing in importance. For this reason the experimental techniques employed in Raman spectroscopy of Na_xWO_3 will be described in some detail in Sec. II. In Sec. III, the temperature-dependent Raman spectra of Na_xWO_3 will be presented. The consistency between the octahedral-tilt space-group assignments for the four phases of Na_xWO_3 and the observed Raman spectra will be established in Sec. IV as a consequence of the selection rules for vibrational Raman scattering that are deduced from these space groups. Furthermore, the soft Raman active external lattice modes of the WO_6 octahedra will be explicitly represented in terms of the eigenvectors of the "positive"-tilt or M-point distortions of the perovskite structure. Section V will be devoted to concluding remarks.

II. EXPERIMENTAL TECHNIQUES

A. Sample preparation

Large single crystals of Na_xWO_3 with $x \geq 0.5$ were grown by electrolysis of the melt,[3] prepared from a charge of reagent grade Na_2WO_4 and WO_3. Low current densities (~ 2 mA/cm^2), uniformity of the melt temperature, and good temperature control (± 2 °C over several days) are imporant factors contributing to optimal growth conditions. Single-crystal nucleation and growth could be achieved by seeding or by drawing the cathode wire slightly up into its sheath. Without such precautions, intergrown clusters of small crystals usually form.

The x values were determined to an accuracy ± 0.01 by atomic absorption spectroscopy. For this purpose Na_xWO_3 was decomposed by fusion with spectral grade Li_2CO_3 (low-Na content). The x determination was repeated at least once for each batch of crystals to insure consistency of the results. In good agreement with the results of Shanks,[3] the final value of x could be estimated closely from the starting Na_2WO_4 mol.%.

It is worthwhile to comment on the growth habit and cleavage properties of the single crystals, observed in the present study as a function of sodium concentration. A crystal for which $x=0.5$ is deep violet in color and grows—under proper conditions—as a perfect dodecahedron, i.e., a cubic crystal exhibiting only (110) faces. Increasing x causes (100) faces to develop. Thus, the forms ({110}) and ({100}) coexist up to $x\sim 0.55$ (red-purple in color) which exhibits (100) faces only. Samples with $x>0.55$ grow in the shape of cubes. Empirically we find that the change in growth habit of Na_xWO_3 below $x=0.6$ coincides with changes in the intrinsic properties of the crystals, as evidenced by the absence of a tetragonal phase at any temperature in the sample with $x=0.52$.[29] Furthermore, the cubic crystals can be cleaved with a razor blade along (100) cleavage planes, but the ease with which they can be cleaved, as well as the smoothness of the cleaved surfaces, decreases as x is decreased. For $x<0.6$ the crystals do not cleave at all.

B. Measurements

Raman spectra of Na_xWO_3 single crystals were recorded in the Brewster angle backscatter geometry. Initially, spectra were excited with both $\lambda_0=5145$ Å and $\lambda_0=4880$ Å Ar^+ laser lines. A double holographic grating scanning monochromator, GaAs phototube RCA 31034*A*, and photon counting electronics were employed. These have been described in detail elsewhere.[30] Spectra were typically recorded with a spectral slit width of 8 cm^{-1}. Because our samples were metallic, the pseudobackscattering configurations *HH* and *HV* approximated true backscatter geometry, i.e., $HH\approx\bar{z}(yy)z$ and $VH\approx\bar{z}(xy)z$. *H* and *V* denote polarization directions parallel (*H*) and perpendicular (*V*) to the scattering plane; here the polarization configuration is specified by the standard $x_i(x_jx_k)x_l$ notation.[31]

For measurements at cryogenic temperatures, samples were bonded to an OFHC copper block with silver epoxy (Emmerson and Cummings Eccobond 58-*C*) and mounted in the optical sample chamber of a liquid-He throttling Dewar. The temperature of the block was read with a calibrated silicon diode, and temperature control was provided by means of a small heater winding to which current was fed by a standard bridge circuit. At high temperatures (300–600 K) samples were held by a gentle suction to a tiny hole drilled in the base of a hollow aluminum cylinder. This technique avoided the outgasing and curing problems posed by high-temperature cements. The cylinder was wound with heating wire and mounted in a glass optical cell that was continually flushed with He gas. Chromel-alumel thermocouple junctions in contact with the sample and winding were used for temperature measurement and control, respectively. Temperatures were controlled to ± 0.1°C.

Raman spectroscopy of metals is technically difficult because the interaction of visible light with a metal whose conductivity is σ is usually confined to the classical skin depth at the frequency ω of the laser excitation. For a good conductor, $\delta=c\times(2\pi\sigma\omega)^{-1/2}$ below the plasma edge (in Cu, $\delta\leq 100$ Å at $\lambda_0=5000$ Å). However, as noted by Scott *et al.*,[8] the free-electron density, n, in sodium-tungsten bronzes is such that the plasma frequency $\omega_p=(4\pi ne^2/m^*)^{1/2}$ is found in the visible, resulting in a sharp decrease in the reflectivity R and an order of magnitude increase in penetration depth for visible light near ω_p. Here m^* is the electron effective mass. Figure 4 shows the behavior of the normal reflectance R in the visible, as observed independently by Scott,[8] Lynch,[6] Fujeida,[5] and others. These authors observed that the x dependence of the curve R—upshift in the position of $E(R_{\min})$ with increasing x—accounts for the dramatic color variation of sodium-tungsten bronze crystals from violet ($x=0.5$) to red ($x=0.6$) to orange ($x=0.7$) to gold ($x=0.8$). Using the optical data for $x=0.65$ reported by Lynch *et al.*, a calculation of the absorption coefficient $\alpha=2k\omega/c$ at $E(R_{\min})=2.3$ eV yields a value of $\alpha=6\times 10^4$ cm^{-1}. Here $k=\mathrm{Im}N$, where N is the complex dielectric constant.

Clearly this increased penetration near ω_p is important for light scattering. The Na concentration dependence of the reflectivity and penetration depth

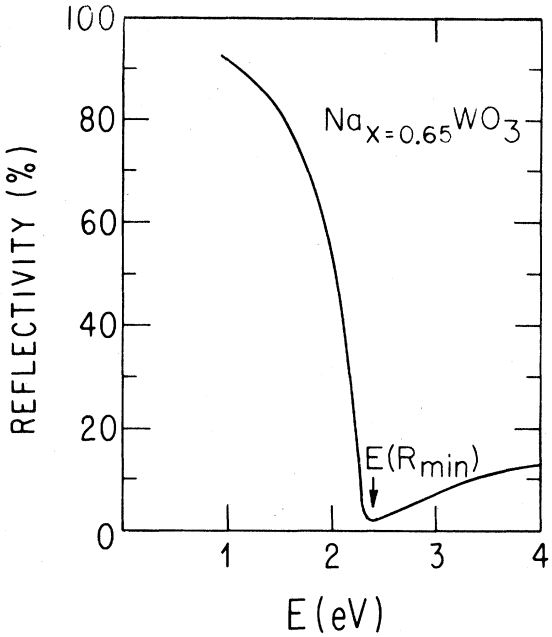

FIG. 4. Reflectivity for $Na_{x=0.65}WO_3$ (normal incidence).

implies that Raman scattering will be enhanced in Na_xWO_3 crystals in which the reflectivity minimum is "concentration tuned" to the laser frequency. In fact, we found that Raman intensities decreased by an order of magnitude with decreasing concentration over the range $0.94 > x > 0.52$ in measurements performed with a fixed laser line, $\lambda_0 = 5145$ Å.

These results suggest the use of a laser source tunable in the visible for the sake of maximizing the Raman signal by maximizing the interaction volume of the radiation and sample. However, in spite of the metallic conductivity and opacity of these materials to visible light, the most serious experimental limitation was not the absolute Raman scattering intensity, but rather the *masking* of the Raman signal by intense parasitic scattering. Unshifted scattered light reflected into the monochromator by imperfections of the sample surface, referred to as parasitic scattering, gives rise to a stray light signal and apparent broadening of the laser line that inhibits the ability of the monochromator to resolve spectral features in the low-frequency region ($\omega < 200$ cm^{-1}). This problem is universally encountered in Raman and Brillouin spectroscopy of opaque materials, but is especially detrimental in a light scattering study of second-order phase transitions where Raman active soft-mode features emerge near $\Delta\omega = 0$.

Removal of surface imperfections by chemical or mechanical polishing often suffices to overcome the problem of parasitic scattering. In the present case however, the vibrational spectra of Na_xWO_3 were observed to be extraordinarily sensitive to surface preparation. It was found that surfaces of optical quality in Na_xWO_3 single crystals could be obtained only at the expense of loss of reproducibility of the Raman data. While no procedure for etching or electropolishing Na_xWO_3 could be found that produced a smooth surface—a manifestation of the high degree of inertness of these materials—mechanical polishing with 50 Å alumina powder seriously and irreversibly damaged the surface layers: the strains induced could only partially be removed by annealing.

In lieu of polishing the sample surface, the unshifted scattered light can be attenuated relative to the inelastically scattered component by inserting an iodine filter[32] in the collection optics. The iodine filter consists of a cylindrical glass cell containing crystals of iodine. The vapor pressure of the iodine inside the cell can be changed by heating the cell. With an intracavity etalon, an Argon ion laser can be tuned to a single longitudinal mode near 5145 Å that is resonantly absorbed by the iodine vapor. Therefore elastically scattered light within the 700-MHz bandwidth of the iodine absorption that would otherwise enter the monochromator is selectively filtered out by the iodine cell. In the present experiments, Raman data were obtained from (100) cleaved single-crystal platelets of Na_xWO_3 having surfaces of

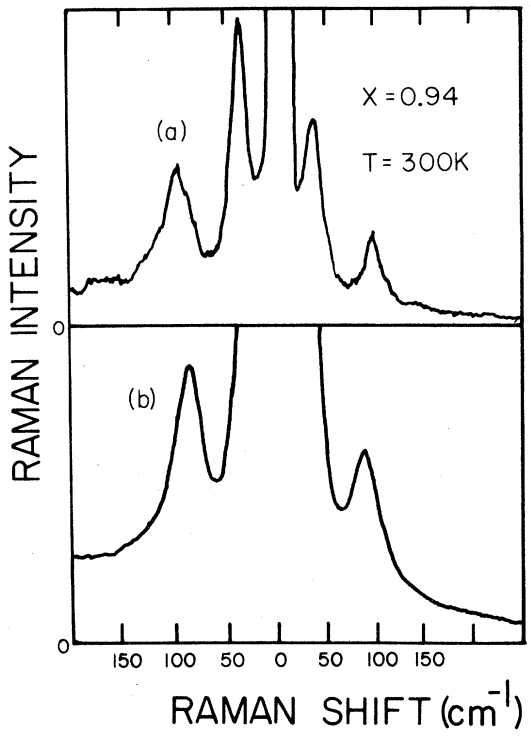

FIG. 5. Raman spectra for $x = 0.94$ recorded (a) with and (b) without the iodine filter. Note that the low-frequency feature at $\omega = 40$ cm^{-1} cannot be discerned in spectrum (b).

poor optical quality, but which were taken to be unstrained as evidenced by the reproducibility of the Raman spectra with respect to temperature cycling. The iodine filter was kept at the relatively high temperature of about 80° C. At this temperature, the optical density of the cell away from resonance incurred ~50% loss of Raman signal, but reduced the parasitic component by a factor of $\sim 10^6$. Consequently, spectra could be recorded in the low-frequency region down to wave number shifts as low as 4 cm^{-1}. The effect of the iodine cell is illustrated dramatically by the spectra of Fig. 5, wherein the Raman spectra for $x = 0.94$, recorded at room temperature with and without the iodine cell, are shown together for comparison. The Raman line at $\omega \approx 40$ cm^{-1} is clearly resolved in the spectrum recorded with the iodine filter, Fig. 5(a), while in Fig. 5(b), the presence of the low-frequency mode cannot be discerned.

III. EXPERIMENTAL RESULTS

Some of the Raman spectra to be reported in this section have appeared in a previous publication.[16] However, these data will be reproduced here as part of a more complete presentation of the light scattering data for Na_xWO_3. In the present section, the ex-

perimental evidence provided by Raman spectroscopy for the sequence of structural phase transitions in Na_xWO_3, which occur at the transition temperatures $T_U(x)$, $T_M(x)$, and $T_L(x)$ will be presented, while the selection rules for first-order Raman scattering in Na_xWO_3, whereby the observed Raman bands and their polarization properties can be correlated with the proposed structural assignments for the four phases of Na_xWO_3, will be established in Sec. IV.

For a given value of x in the concentration range $0.62 \leq x \leq 0.94$ the Raman spectrum of Na_xWO_3, at temperatures $T < T_M(x)$, consists of two discrete, Raman-active soft modes, superposed on an inelastic scattering continuum, which emerge successively with decreasing temperature as the sample temperature crosses the phase boundaries at $T = T_U(x)$ and $T = T_M(x)$ from above. The upper transition temperature $T_U(x)$ has been detected in the x-ray data of Clarke by a splitting of the lattice parameters a_p, b_p, c_p as the temperature is decreased below $T = T_U$, such that

$$a_p = b_p = c_p, \quad T > T_U \ ,$$

$$a_p = b_p < c_p, \quad T < T_U \ .$$

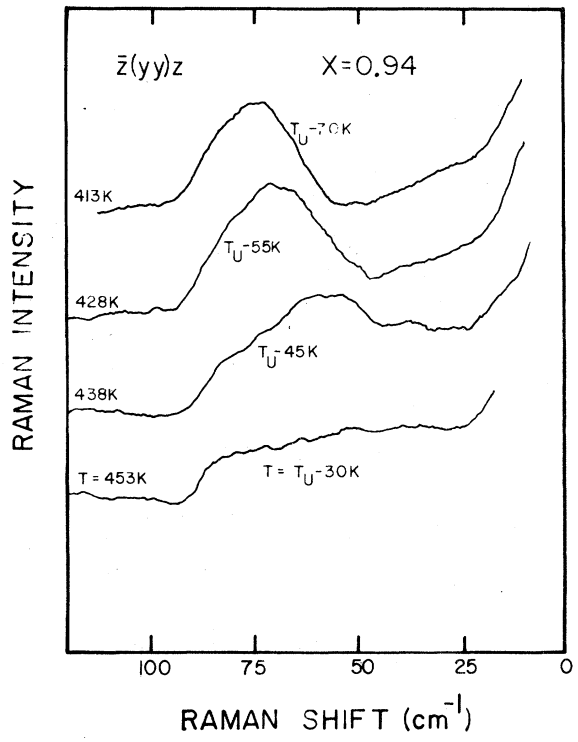

FIG. 6. Raman spectra for $x = 0.94$ as $T = T_U$ is approached from below. Note that the single, polarized Raman band $\omega_u(T)$ is severely damped 30 K below the transition temperature $T_U = 483$ K. The apparent structure in the spectrum with $T = 453$ K, i.e., the "dip" at $\omega \sim 80$ cm^{-1}, is due to absorption by the iodine filter.

This splitting was shown to be continuous at $T = T_U$, and therefore attributable to a second-order structural transition. In the corresponding temperature range, the Raman spectra in Fig. 6 show for $x = 0.94$ the evolution of a single Raman-active soft mode which shifts monotonically to higher energy as the temperature is decreased below $T = T_U$ ($x = 0.94$) $= 483$ K. Using the iodine cell technique we were prepared to record the behavior of the soft mode in the low-frequency region; however, Fig. 6 also shows the severe overdamping of the soft mode as the high-temperature transition is approached from below, whereby the soft-mode intensity diminished to zero well in advance of the transition temperature at finite energy. Thus for $T \geq T_U - 20$ K only background scattering could be observed. The presence of the Raman-active soft mode for $T < T_U$ is characteristic of a second-order displacive transition, in accord with Clarke's measurements and in analogy with ferroelectric soft-mode phase transitions.[19] At a lower temperature $T = T_M(x = 0.94) = 393$ K, the proposed first-order phase transition $a^0a^0c^+ - a^0b^+b^+$, evidenced in x-ray data[17] by a discontinuous splitting of the lattice parameters such that

$$a_p = b_p < c_P, \quad T > T_M \ ,$$

$$a_p < b_p = c_p, \quad T < T_M \ ,$$

was found to coincide with the abrupt emergence of a second Raman-active soft mode at low frequency $\omega \approx 35$ cm^{-1}, as can be seen in Fig. 7 wherein Raman

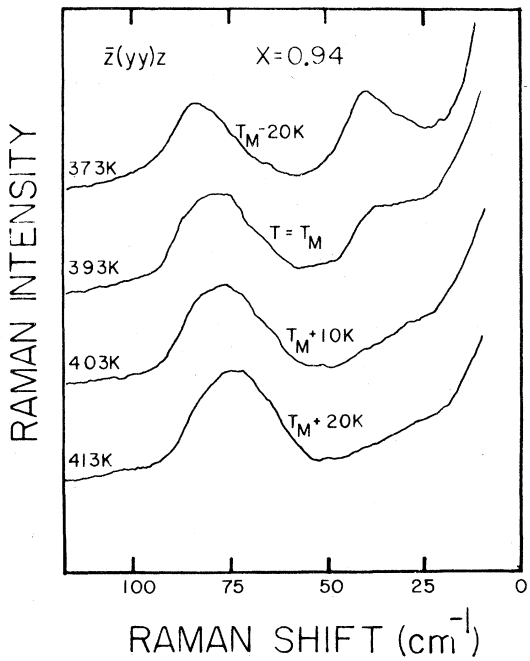

FIG. 7. Raman spectra for $x = 0.94$ with $T_M + 20$ K $> T > T_M - 20$ K. Note the emergence of the low-frequency soft mode $\omega_l(T)$ at $T = T_M$.

spectra recorded in the temperature interval ($T_M - 20$ K, $T_M + 20$ K) document the appearance of the new mode. Thus, for $T < T_M$, the Raman spectrum of Na_xWO_3 with $x = 0.94$ exhibits two Raman-active soft modes that shift to higher frequency as the temperature is decreased. To the high-frequency member and low-frequency member of the soft-mode pair we will ascribe the temperature-dependent frequency $\omega_u(T)$ and $\omega_l(T)$, respectively. The Raman spectra that appear in Fig. 8 span the temperature range $3 < T < 500$ K. For $T < T_M = 343$ K, the two soft modes are present in the Raman spectra, and it is evident that $\omega_u(T)$ and $\omega_l(T)$ increase as the temperature is lowered from room temperature down to

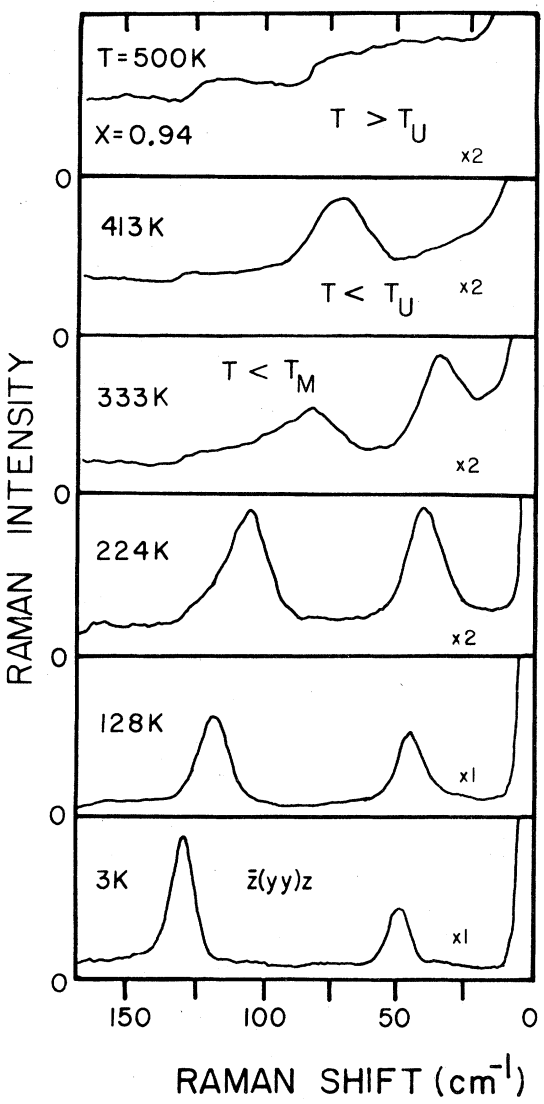

FIG. 8. Spectra for $x = 0.94$ than span the temperature range $3 < T < 500$ K. Discrete Raman bands are absent for $T = 500$ K. The "dips" in the continuum are due to absorption by the iodine filter.

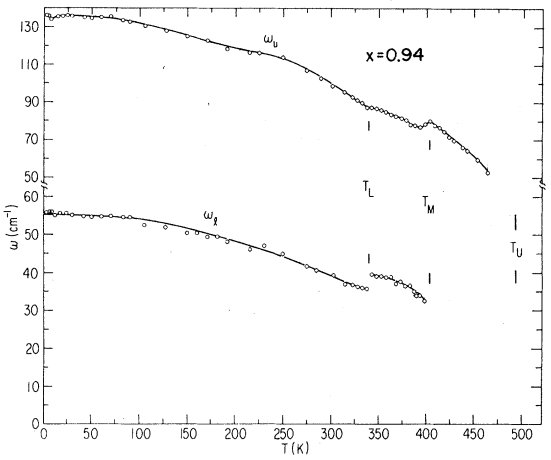

FIG. 9. Plot of $\omega_u(T)$ and $\omega_l(T)$ for $x = 0.94$, $3 < T < 500$ K.

3 K. However, in Fig. 9 a detailed plot of $\omega_u(T)$ and $\omega_l(T)$ for $3 < T < 500$ K shows the occurrence of a *stepwise discontinuity* $\Delta\omega_l(T = T_L) \approx 4$ cm^{-1} at the temperature $T = T_L(x = 0.94) = 343$ K, which coincides with the proposed first-order transition $a^0b^+b^+ - a^+a^+a^+$ where

$$a_p < b_p = c_p, \quad T > T_L \ ,$$

$$a_p = b_p = c_p, \quad T < T_L \ .$$

Furthermore the upper curve $\omega_u(T)$, while apparently continuous across the first-order transition temperatures T_L and T_M, exhibits at each of these temperatures a definite "kink" or discontinuity of slope.

The low-temperature Raman spectra in Fig. 10 for $x = 0.94$, 0.81, 0.72, and 0.62 exhibit for each value of x a soft-mode pair $\omega_u(T)$ and $\omega_l(T)$. Evidently each member of the soft-mode pair is shifted to lower frequency as the sodium concentration is decreased. In addition, the Raman bands $\omega_u(T)$ and $\omega_l(T)$ are polarized, with typical depolarization ratios $\rho \approx 0.05$. Representative depolarization data for $x = 0.94$ and $T = 50$ K are shown in Fig. 11. For all x values studied and for all temperatures $T < T_U(x)$, only diagonally polarized Raman modes could be detected.

It is to be emphasized that for each sodium-tungsten bronze sample studied with x in the range $0.6 < x < 1$, the soft-mode pair $\omega_u(T)$ and $\omega_l(T)$ was observed to evolve as a function of decreasing temperature exactly in the manner described above for $x = 0.94$, except that the values of T_U, T_M, and T_L depend on x.

In concluding the presentation of the Raman scattering results for Na_xWO_3 with $0.6 < x < 1$, it is important to recall that the Raman-active soft modes are superposed on an inelastic continuum. The back-

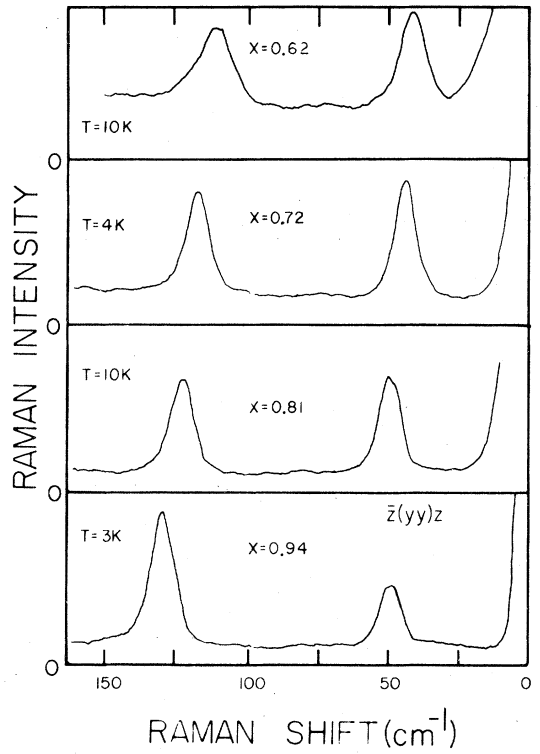

FIG. 10. Low-temperature Raman spectra of "cubic" Na_xWO_3 with $0.6 < x < 1$, recorded with the iodine filter. The abscissa is linear in wavelength rather than in wave number.

ground scattering is real, as opposed to a stray light signal. This point is verified in Fig. 12 in which the low-temperature spectrum for the sample with $x = 0.81$ exhibits no anti-Stokes scattering. While no discrete Raman lines are observed in the Raman spectrum of Na_xWO_3 at temperatures $T > T_U(x)$, the

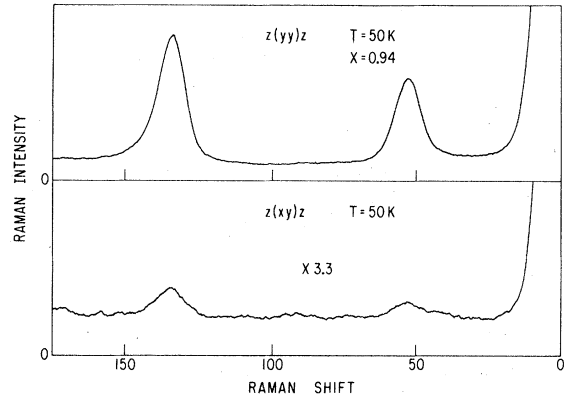

FIG. 11. Typical depolarization data. The Raman bands $\omega_u(T)$ and $\omega_l(T)$ (at high and low frequency, respectively) were strongly polarized at all temperatures. Here $\rho \approx 0.07$ for both bands.

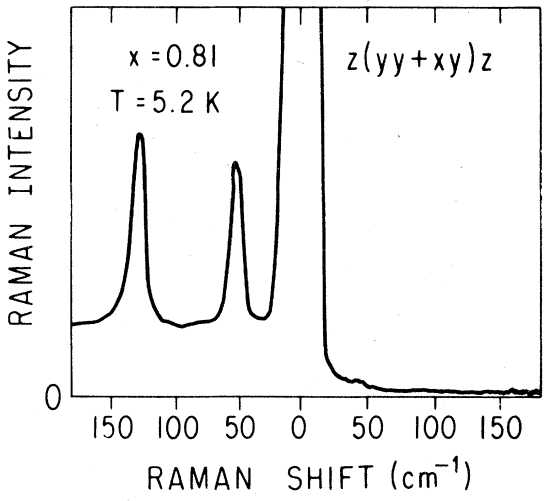

FIG. 12. Low-temperature spectrum for $x = 0.81$. Note that the background or continuum scattering is absent in the anti-Stokes spectrum.

background scattering is present and grows in intensity as the temperature of the sample is raised.

IV. DISCUSSION

A. Raman-scattering selection rules

The lattice-dynamical information provided by Raman scattering is obtained to a first approximation by enumerating the Raman-active lattice vibrations of the crystal being studied. The group-theoretical selection rules for Raman scattering in a crystalline material are based on the harmonic description of the lattice vibrations,[33–35] with the added condition that only the long-wavelength vibrations belonging to $\vec{k} = 0$ (i.e., modes at the Brillouin-zone center) can appear in the first-order Raman spectrum. For a perfect crystal the condition that first-order Raman scattering occurs only at the zone center is a consequence of wave vector conservation,[36] i.e.,

$$\vec{k}_i = \vec{k}_s + \vec{k}_p \ . \tag{5}$$

Here $\vec{k}_i$ and $\vec{k}_s$ are the incident and scattered photon wave vectors, and $\vec{k}_p$ is the wave vector of the phonon that is created (destroyed) in the Stokes (anti-Stokes) scattering process. Breakdown of the $\vec{k} = 0$ selection rule can be observed in Raman scattering from amorphous solids[37] or in scattering from microcrystallites whose linear dimensions L are much smaller than the wavelength of the incident light, such that the uncertainty in the phonon wave vector Δk_p obeys[38]

$$L \Delta k_p \sim 1 \ .$$

Although the $\vec{k} = 0$ rule is exact only in the case of

an infinite, perfectly ordered crystal, in which the phonon coherence range is infinite, this rule remains an excellent approximation in Raman scattering from crystals of finite size which contain roughly a number of primitive cells $N \gtrsim 10^2$ or 10^3. However, in the case of crystals with random defects or vacancies, as is the case in the solid solution Na_xWO_3, disorder-induced breakdown of wave vector conservation may or may not be observed in practice. The effect of chemical disorder, or disorder due to defects can best be evaluated in a structure in which Raman scattering is first-order forbidden (in the absence of vacancies or defects), such as the NaCl structure or the undistorted ABO_3 perovskite structure wherein every atom occupies a center of inversion symmetry. In the case of the transition-metal carbide TiC_x, which has the NaCl structure, Klein *et al.*,[39] have shown that the carbon vacancies in samples with $x=0.8$, 0.9, 0.97 give rise to a nonzero polarizability derivative $(\partial\rho/\partial u)_{u=0}$ for certain motions of the atoms near the vacancy site, thereby inducing first-order Raman scattering that is roughly proportional to the one-phonon density of states. The Raman spectra in TiC_x consist of several broad features attributable to a convolution of contributions to the one-phonon scattering from accoustic (low-energy) and optic (high-energy) phonons of wave vector $\vec{k}$, where $\vec{k}$ ranges over the entire Brillouin zone. In contrast, the Raman spectra of the solid solutions Na_xWO_3 exhibit discrete one-phonon excitations which can be accounted for without invoking arguments pertaining to disorder-induced scattering. Neglecting the nonstoichiometry of Na_xWO_3, one can understand immediately the absence of the discrete Raman lines for $T > T_U(x)$, consistent with the ideal perovskite structure of the high-temperature phase. Likewise, as will be shown below, a consideration of the average structure, i.e., that of the WO_3 host lattice, suffices to explain the soft vibrational excitations which arise in each of the three distinct phases that obtain for $T < T_U(x)$. The continuum background, on the other hand, cannot be associated with phonons, primarily because the background intensity increased much more rapidly with rising temperature than did the first-order soft-mode Raman lines which must exhibit Stokes intensities proportional to $n+1$. Furthermore, the continuum spectrum exhibited by unpolished samples of Na_xWO_3 was flat and featureless, extending in frequency out to ~ 4000 cm^{-1}. The temperature dependence, the featureless profile and the frequency range of the continuum scattering are not characteristic of a one- or two-phonon density of states. Interband electronic scattering is the most likely source of the background.

Considering the absence of identifiable disorder-induced scattering in the Raman spectra of unpolished samples, the most significant manifestation of the chemical disorder in Na_xWO_3 appears to be a broadening of Raman lines due to spatial variation of the sodium concentration. The incident light in effect samples all possible microscopic configurations of randomly distributed sodium ions in the material; therefore, an observed Raman band constitutes a convolution or ensemble average of scattering contributions from these configurations, in which the force constants and frequencies associated with the Raman-active vibration vary with the local value of x. In Fig. 13 the width of the Raman-active soft mode $\omega_u(T)$ at 10 K has been plotted as a function of x. While these bands exhibit overall a systematic broadening with decreased sodium concentration, a dip in the curve Γ (FWHM) vs x occurs near $x=0.75$. This result suggests the possibility of ordering of the sodium atoms in the concentration range near $x=0.75$, whereby the microscopic homogeneity associated with the ordering gives rise to a narrowing of the Raman lines.

It has been assumed above that the light scattering spectra are characteristic of the bulk material; although not obvious, this seems to be true on several counts. Firstly, the transition temperatures for the phase transitions of the bulk determined by x-ray diffraction and by light scattering, respectively, were in good agreement, especially for the sharply defined first-order transitions at the temperatures $T_M(x)$ and $T_L(x)$. Secondly, at fixed temperature the Raman shifts $\omega_u(T)$ and $\omega_l(T)$ did not depend

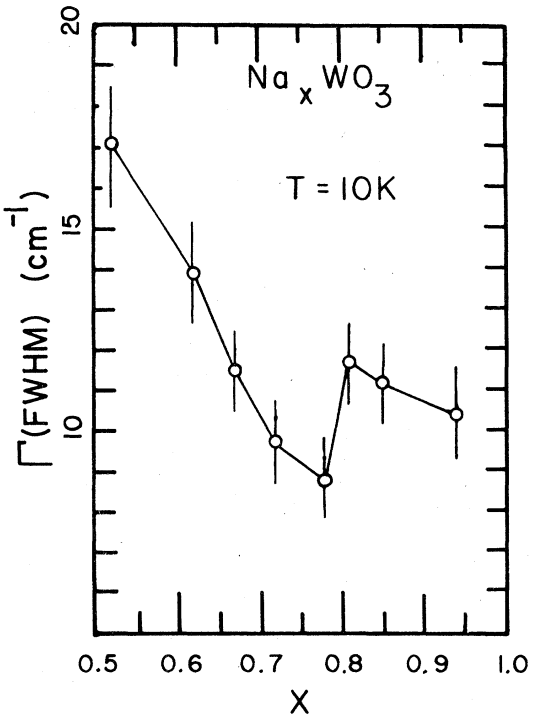

FIG. 13. FWHM vs x for the Raman band ω_u ($T=10$ K).

on the laser frequency, i.e., the laser penetration depth. Thus, it was established that the surface region in which the x value is significantly lower than that of the bulk does not contribute appreciably to the Raman spectra; the sodium-depleted layer is probably shallow compared to the laser penetration depth. Indeed, Auger studies of Na_xWO_3 samples—including anodized samples—have indicated a concentration profile in which the x value reaches that of the bulk within a few hundred angstroms of the surface.[40]

The interpretation of the Raman spectra will be based on the following determination of the $\vec{k}=0$ vibrations of the proposed rigid-tilt structures of Na_xWO_3. At the same time, the validity of these structural assignments will be subject to a comparison of the predicted Raman activity in each phase with the experimental results. In the following, P_0 denotes the point group of the wave vector $\vec{k}=0$; R is a symmetry operation that belongs to P_0; $G_s \subset P_0$ is the site group of a particular equivalent set of atomic sites; ϕ and σ label irreducible representations of P_0 and G_s, respectively; $D^p(R)$ is the polar vector representation. Confining our attention to a particular equivalent set of n atoms in the primitive cell, let $u_{i,\alpha}$ denote a unit displacement of atom i in the direction $\alpha=x,y,z$. The transformation from the $3n$ basis vectors $u_{i,\alpha}$ which generates the mechanical representation of P_0, to symmetry vectors $\vec{b}^{\phi,l,r}$ $(\vec{k}=0)$, yields a reduction of the mechanical representation on the crystal point group P_0: The symmetry vector $\vec{b}^{\phi,l,r}$ $(\vec{k}=0)$ belongs to the rth repetition of the IR (irreducible representation) ϕ of dimension l_ϕ, this IR having occurred a number of times n_ϕ. If $l_\phi > 1$, the index l labels the several basis vectors for the irreducible representation ϕ. Via the correlation method,[41] the numbers n_ϕ can be determined

$$n_\phi = \sum_\sigma a_{\phi\sigma} n_\sigma \ . \tag{6}$$

Here the numbers $a_{\phi\sigma}$ and n_σ arise from the reduction of ϕ and $D^p(R)$ on the site group G_s

$$\chi^\phi(R) = \sum_\sigma a_{\phi\sigma}\chi^\sigma(R) \tag{7}$$

and

$$\mathrm{Tr}\, D^p(R) = \sum_\sigma n_\sigma \chi^\sigma(R) \ . \tag{8}$$

The total number of lattice vibrations that transform as the species ϕ is the sum of contributions n_ϕ from each of the several sets of equivalent atoms in the primitive cell. In Table II, the $\vec{k}=0$ vibrations

TABLE II. Symmetry species of $\vec{k}=0$ lattice vibrations in Na_xWO_3 otahedral tilt structures.

I. $T > T_U$ $a^0a^0a^0(O_h^1)$, $Z_0=1$:

(a) 1 W, O_h; (b) 3 O, D_{4h}

$$T(\vec{k}=0,O_h) = 3F_{1u} + F_{2u}$$

II. $T_M < T < T_U$ $a^0a^0c^+(D_{4h}^5)$, $Z_0=2$:

(a) 2 W, C_{4h}; (b) 2 O, C_{4h}; (c) 4 O, C_{2v} (C_2'')

$$T(\vec{k}=0,D_{4h}) = A_{1g}(\alpha_{xx}+\alpha_{yy},\alpha_{zz}) + B_{1g}(\alpha_{xx}-\alpha_{yy}) + A_{2g} + B_{2g}(\alpha_{xy}) + E_g(\alpha_{xz},\alpha_{yz}) + 2A_{1u} + 3A_{2u} + B_{1u} + 6E_u$$

III. $T_L < T < T_M$ $a^0b^+b^+(D_{4h}^{17})$, $Z_0=4$:

(f) 4 W, $C_{2h}(C_2'')$; (h) 4 O, C_{2v} (C_2''); (n) 8 O, $C_s(\sigma_v)$

$$T(\vec{k}=0,D_{4h}) = 3A_{1g}(\alpha_{zz}+\alpha_{yy},\alpha_{xx}) + 2A_{2g} + 2B_{2g}(\alpha_{zy}) + 3B_{1g}(\alpha_{zz}-\alpha_{yy}) + 4E_g(\alpha_{zx},\alpha_{yx}) + 2A_{1u} + 5A_{2u} + 3B_{1u} + 4B_{2u} + 8E_u$$

IV. $T < T_L$ $a^+a^+a^+(T_h^5)$, $Z_0=4$:

(c) 4 W, C_{3i}; (g) 12 O, C_s

$$T(\vec{k}=0,T_h) = 2A_g(\alpha_{xx}+\alpha_{yy}+\alpha_{zz}) + 2E_g(\alpha_{xx}+\alpha_{yy}-2\alpha_{zz},\alpha_{xx}-\alpha_{yy}) + 4F_g(\alpha_{xy},\alpha_{yz},\alpha_{zx}) + 2A_u + 2E_u + 8F_u$$

are enumerated for each of the rigid tilt structures in Na_xWO_3 proposed by Clarke. The numbers n_ϕ were calculated using the site group information that is given explicitly in Table II by Wyckoff notation for the site, the corresponding Schoenflies symbol for the site group and the number of W or O atoms in each equivalent set.[42] These site group assignments were deduced by imposing on the ideal perovskite structure the "positive" tilt lattice distortions $a^0a^0c^+$, $a^0b^+b^+$, and $a^+a^+a^+$. Projection drawings of the rigid tilt crystal structures thus obtained are found in Fig. 14. Finally, in Table II the polarizability components are given in parentheses next to the irreducible representations of P_0 which they generate.[36]

The group-theoretical selection rules which have been deduced from the proposed rigid tilt space-group assignments $a^0a^0a^0$ (O_h^1), $a^0a^0c^+$ (D_{4h}^5), $a^0a^0b^+$ (D_{4h}^{17}), $a^+a^+a^+$ (T_h^5) are completely consistent with the experimental observations in Raman scattering with respect to the number and polarization properties of the Raman lines. We recall that the two discrete Raman bands labeled $\omega_u(T)$ and $\omega_l(T)$ were found to be strongly polarized. The bands $\omega_u(T)$ and $\omega_l(T)$ can be accounted for among the zone center vibrations of the low-temperature cubic phase $a^+a^+a^+$ ($T < T_L$) that have Raman tensors with diagonal elements. These are

$$2A_g(\alpha_{xx}+\alpha_{yy}+\alpha_{zz})+2E_g(\alpha_{xx}+\alpha_{yy}-2\alpha_{zz},\ \alpha_{xx}-\alpha_{yy}) .$$

Similarly, in the temperature range $T_L < T < T_M$, the presence of the polarized Raman bands $\omega_l(T)$ and $\omega_u(T)$ is consistent with the group-theoretical predictions in Table II, where the polarized modes

$$3A_{1g}(\alpha_{zz}+\alpha_{yy},\alpha_{xx})+3B_{1g}(\alpha_{zz}-\alpha_{yy})$$

comprise 6 of the 12 Raman active vibrations of the two-tilt, tetragonal phase $a^0b^+b^+$. The band $\omega_l(T)$ is absent at temperatures above the $a^0b^+b^+$-$a^0a^0c^+$. transition. However the two polarized vibrations

$$A_{1g}(\alpha_{xx}+\alpha_{yy},\alpha_{zz})+B_{1g}(\alpha_{xx}-\alpha_{yy})$$

of the one-tilt structure $a^0a^0c^+$ allow for the presence of the single, strongly polarized soft mode $\omega_u(T)$ that is observed in the temperature interval $T_M < T < T_U$. No Raman-active modes should appear in the ideal perovskite structure $a^0a^0a^0$; indeed, the Raman spectrum of Na_xWO_3 recorded when $T > T_U$ has been characterized by the absence of discrete, first-order vibrational features.

The consistency between our experimental data and the selection rules in Table II demonstrated above is the extent to which Raman spectroscopy serves as a test of the validity of the rigid tilt space-group assignments in Na_xWO_3. However, it is at first disturbing that many more Raman-active modes were predicted than were observed. Because one-phonon Raman lines seem to be absent outside of the low-frequency region $0 < \omega < 150$ cm^{-1} it can be concluded that the external lattice modes $\omega_u(T)$ and $\omega_l(T)$ exhibit Raman scattering efficiencies that must dominate by a factor of $\sim 10^2$ or greater the scattering due to higher-frequency excitations that, in fact, could not be resolved from the background continuum.

The key to understanding these results lies in the relationship between the soft lattice vibrations and the structural phase transitions encountered here.

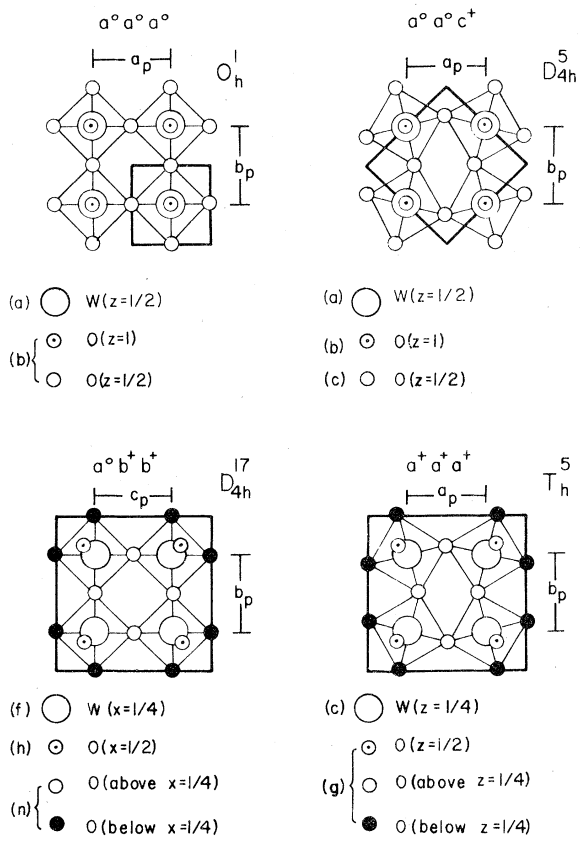

FIG. 14. Projections of the rigid tilt structures of Na_xWO_3. The heavy lines are the boundaries of the smallest unit cell with edges that are orthogonal. For $a^0a^0a^0$ and $a^0a^0c^+$ this unit cell is primitive. For $a^0b^+b^+$ and $a^+a^+a^+$ it is not primitive.

B. Application of the Landau theory

The further interpretation of the Raman data depends first on the assumption that the proposed space-group assignments for Na_xWO_3 are correct, and second, on the observation that each of the rigid tilt space groups $D_{4h}^5(a^0a^0c^+)$, $D_{4h}^{17}(a^0b^+b^+)$, and $T_h^5(a^+a^+a^+)$ is a subgroup of the space group O_h^1 of the ideal perovskite structure. The significance of

this latter observation derives from the phenomenological Landau theory of crystallographic phase transitions. It follows from the relations $D_{4h}^5 \subset O_h^1$, $D_{4h}^{17} \subset O_h^1$, and $T_h^5 \subset O_h^1$, and additional criteria of the Landau theory which govern the mutual compatability of space groups which may be realized above and below the critical temperature T_U in a second-order structural phase transition, that each of the following crystallographic transformations may proceed via a second-order displacive phase transition

$$\begin{aligned} &a^0a^0a^0 \rightarrow a^0a^0c^+ \ , \\ &a^0a^0a^0 \rightarrow a^0b^+b^+ \ , \\ &a^0a^0a^0 \rightarrow a^+a^+a^+ \ . \end{aligned} \tag{9}$$

Conversely $D_{4h}^{17} \not\subset D_{4h}^5$ and $T_h^5 \not\subset D_{4h}^{17}$, whereby $a^0a^0c^+ \rightarrow a^0b^+b^+ \rightarrow a^+a^+a^+$ are first-order transitions. The order parameter in any second-order displacive transition is a set of atomic displacements that transform according to the identity representation of the ordered phase; for $T < T_U$ these displacements are proportional to the eigenvector displacements of a Raman-active lattice vibration. Ordinarily this lattice vibration is the symmetric soft mode whose frequency approximately obeys

$$\omega(A_{1g}) \propto (T_U - T)^{1/2} \ . \tag{10}$$

However, if the order parameter displacements are associated with the simultaneous softening and condensation of *two or more* degenerate vibrations of the high-temperature phase, then more than one soft mode may emerge in the Raman spectrum for $T < T_U$. A simple model of the phase transition incorporates a free-energy function F that depends on two independent degrees of freedom u and v

$$F = a(u^2+v^2) - b(uv) + c_0(u^4+v^4) \ , \tag{11}$$

where

$$a = a_0(T - T_U); \quad b = b_0(T - T_U) \ ; \quad a_0, b_0, c_0 > 0 \ .$$

When $T < T_U$, $F(u = u_0, v = v_0)$ is an absolute minimum for

$$u_0 = v_0 = \{[(2a_0 - b_0)/4c_0](T_U - T)\}^{1/2} \tag{12}$$

provided $b_0 < a_0$, while the curvature of the function F is proportional to the square of the frequency of oscillations about the minimum. Let ω_1 and ω_2 denote the frequencies of oscillations corresponding to the initial small displacements $(u_0+\epsilon, v_0+\epsilon)$ and $(u_0+\epsilon, v_0-\epsilon)$, respectively. Then

$$\begin{aligned} \omega_1 &= 2[(2/m)(a_0 - b_0/2)(T_U - T)]^{1/2} \ , \\ \omega_2 &= 2[(2/m)(a_0 - b_0)(T_U - T)]^{1/2} \ , \end{aligned} \tag{13}$$

where m is the mode mass. Adapting this model to a structural phase transition, we let c_1 and c_2 (corresponding to u and v) be the net-time average of the atomic displacements $\vec{u}_1(t)$ proportional to the degenerate eigenvectors $\vec{b}_1(\vec{k}_1)$ and $\vec{b}_2(\vec{k}_2)$, respectively

$$c_1 = \left\langle \sum_i \vec{u}_i(t) \cdot \vec{b}_1(\vec{k}_1) \right\rangle_{\text{av}} \ . \tag{14}$$

c_2 is defined similarly. Here the index i ranges over all atoms in the primitive cell and the eigenvectors $\vec{b}_1(\vec{k}_1)$ and $\vec{b}_2(\vec{k}_2)$ are linear combinations of symmetry vectors of the same type. Then

$$c_1 = c_2 = \begin{cases} 0, & T > T_U \ , \\ c(T_U - T)^{1/2}, & T < T_U, \quad c > 0 \ . \end{cases} \tag{15}$$

The phase transition is described by a vector order parameter whose components are the amplitudes c_1 and c_2. In fulfillment of the Landau criteria for the second-order phase transition, $\vec{k}_1$ and $\vec{k}_2$ belong to the star of the wave vector $\vec{k}$ such that the group of the wave vector, $G(\vec{k})$, subduces the identity representation of G, the space group of the ordered phase.[43] As a consequence, the reduction of the vector space

$$\{\vec{b}_1(\vec{k}_1), \vec{b}_2(\vec{k}_2)\} \tag{16}$$

on the point group P_0 (for $T < T_U$) will yield the eigenvector $\vec{b}^{A_{1g}}(\vec{k}=0)$ of the completely symmetric soft mode. However, another IR ϕ that is not the identity will also occur. The reduction of the vector space (16) consists of finding the new eigenvectors $\vec{b}^{A_{1g}}$ and $\vec{b}^{\phi}$. These are

$$\begin{aligned} \vec{b}^{A_{1g}}(\vec{k}=0) &= \frac{1}{\sqrt{2}}[\vec{b}_1(\vec{k}_1) + \vec{b}_2(\vec{k}_2)] \ , \\ \vec{b}^{\phi}(\vec{k}=0) &= \frac{1}{\sqrt{2}}[\vec{b}_1(\vec{k}_1) - \vec{b}_2(\vec{k}_2)] \ , \end{aligned} \tag{17}$$

where the new lattice vibrations A_{1g} and ϕ exhibit the soft-mode behavior

$$\begin{aligned} \omega(A_{1g}) &= \omega'(T_U - T)^{1/2} \ , \\ \omega(\phi) &= \omega''(T_U - T)^{1/2} \ . \end{aligned} \tag{18}$$

By inspection of Eq. (13), we expect $\omega'' < \omega'$. We note also that the relation $\omega(A_{1g}) > \omega(\phi)$, for the respective "in phase" and "out of phase" vibrations A_{1g} and ϕ, follows in analogy with Davydov splitting in the vibrational spectrum of two identical, interacting oscillators.

The above described simultaneous softening of degenerate lattice vibrations is realized in Na_xWO_3. In particular, let $\vec{b}_1(\vec{k}_1)$, $\vec{b}_2(\vec{k}_2)$, and $\vec{b}_3(\vec{k}_3)$ represent positive octahedral tilt displacements about x, y, and z, respectively, where $\vec{k}_1$, $\vec{k}_2$, and $\vec{k}_3$ comprise the star of the BZ boundary point M. The $\vec{b}_i(\vec{k}_i)$ generate the zone boundary representation M_3. Then the soft-mode species for a rigid tilt phase

that is described by some combination of nonzero parameters c_1, c_2, and c_3 will be subduced by the manifold

$$\{c_1\vec{b}_1(\vec{k}_1), c_2\vec{b}_2(\vec{k}_2), c_3\vec{b}_3(\vec{k}_3)\} \ . \tag{19}$$

For the case $c_1=c_2=c_3$ $(a^+a^+a^+)$, the reduction of this space is the following:

$$\vec{b}^{A_{1g}}(\vec{k}=0)=\frac{1}{\sqrt{3}}[\vec{b}_1(\vec{k}_1)+\vec{b}_2(\vec{k}_2)+\vec{b}_3(\vec{k}_3)] \ ,$$

$$\vec{b}^{\phi,1}(\vec{k}=0)=\frac{1}{\sqrt{3}}[\vec{b}_3(\vec{k}_3)+\epsilon\vec{b}_1(\vec{k}_1)+\epsilon^2\vec{b}_2(\vec{k}_2)] \ ,$$

$$\vec{b}^{\phi,2}(\vec{k}=0)=\frac{1}{\sqrt{3}}[\vec{b}_3(\vec{k}_3)+\epsilon^2\vec{b}_1(\vec{k}_1)+\epsilon\vec{b}_2(\vec{k}_2)] \ . \tag{20}$$

where $\epsilon=\exp(2\pi i/3)$, and

$$\omega(\phi,1)=\omega(\phi,2)<\omega(A_{1g}) \ .$$

The "extra" soft mode ϕ is doubly degenerate. Although the rigid tilts $a^0a^0c^+$, $a^0b^+b^+$, and $a^+a^+a^+$ occur sequentially in Na_xWO_3, it is now evident that each phase exhibits in its vibrational Raman spectrum the symmetric soft mode A_{1g} and, for $a^0b^+b^+$ and $a^+a^+a^+$, an "extra" soft mode ϕ. It can be easily verified that the eigenvectors $\vec{b}^{\phi}$ [Eq. (17)] and $(\vec{b}^{\phi,1}, \vec{b}^{\phi,2})$ [Eq. (20)] generate the irreducible representations B_{1g} and E_g of the respective crystal point groups D_{4h} and T_h, appropriate to $a^0b^+b^+$ and $a^+a^+a^+$. These results have been summarized in Table III, and in Fig. 15 where the Raman data have been represented schematically. The upper curve $\omega_u(T)$ has been associated with the symmetric soft mode A_{1g}, while the lower curve $\omega_l(T)$ (solid line) is a plot of the temperature dependence of the "extra" soft mode. The dotted curves were not observed; rather, these curves indicated the temperature dependence for the soft modes that would be measured if the "possible second-order transitions" $a^0a^0a^0 \rightarrow a^0b^+b^+$ and $a^0a^0a^0 \rightarrow a^+a^+a^+$ could be by some means induced to proceed directly, without being interrupted by the sequence of phase transitions that otherwise intervenes. The symmetry assignments for the Raman-active soft modes will now be examined in further detail.

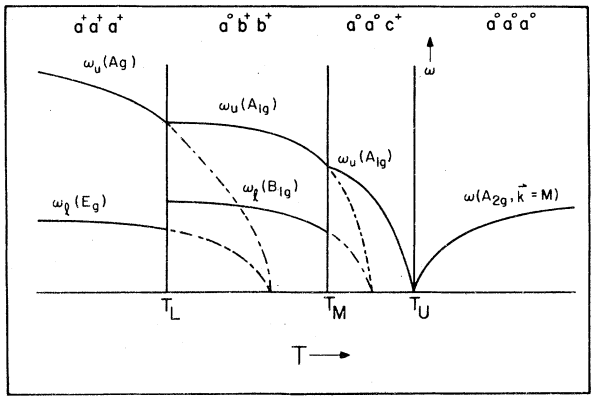

FIG. 15. Schematic representation of the temperature-dependent Raman data. The first-order phase transitions at $T=T_L$ and $T=T_M$ entail a "re-orientation" of the vector order parameter. At $T=T_L$ the curve ω_l is discontinuous.

The results in Table III predict both the number and polarization properties of the soft Raman-active external modes of the WO_6 octahedra, observed in Na_xWO_3. In a single-domain crystal, in the phase $a^0b^+b^+$ $(T_L<T<T_M)$ the Raman lines $A_{1g}(\alpha_{zz}+\alpha_{yy}, \alpha_{xx})$ and $B_{1g}(\alpha_{zz}-\alpha_{yy})$ would be identifiable on the basis of polarization characteristics. Both of these modes are polarized, but B_{1g} should vanish in the scattering configuration $\bar{z}(xx)z$, if the tetragonal axis is parallel to the direction e_x, as can be seen from the Raman tensors

$$A_g: \begin{pmatrix} b & 0 & 0 \\ 0 & a & 0 \\ 0 & 0 & a \end{pmatrix}; \quad B_{1g}: \begin{pmatrix} 0 & 0 & 0 \\ 0 & -c & 0 \\ 0 & 0 & c \end{pmatrix} \ .$$

However, in the Raman measurements the laser

TABLE III. Symmetry of $\vec{k}=0$ soft modes. The soft-mode species are subduced by the manifold of degenerate lattice vibrations of the perovskite structure that transform as M_3.

Phase	Order parameter	Reduction of the space $\{c_1\vec{b}_1(\vec{k}_1), c_2\vec{b}_2(\vec{k}_2), c_3\vec{b}(\vec{k}_3)\}$
O_h^1 $(a^0a^0a^0)$	$c_1=c_2=c_3=0$	. . .
D_{4h}^5 $(a^0a^0b^+)$	$c_1=c_2=0, c_3\neq 0$	$A_{1g}(\alpha_{xx}+\alpha_{yy}, \alpha_{zz})$
D_{4h}^{17} $(a^0b^+b^+)$	$c_1=0, c_2=c_3\neq 0$	$A_{1g}(\alpha_{zz}+\alpha_{yy}, \alpha_{xx})$ $+B_{1g}(\alpha_{zz}-\alpha_{yy})$
T_h^5 $(a^+a^+a^+)$	$c_1=c_2=c_3\neq 0$	$A_{1g}(\alpha_{xx}+\alpha_{yy}+\alpha_{zz})$ $+E_g(\alpha_{xx}+\alpha_{yy}-2\alpha_{zz}, \alpha_{xx}-\alpha_{yy})$

beam was focused on the sample to a line image with approximate area 0.1 mm × 1 mm. Because of the presence of twinned tetragonal domains whose dimensions were smaller than the area of the focused spot, the orientation of the tetragonal axis relative to the laser polarization was not definite. As a consequence, the Raman lines $\omega_u(A_{1g})$ and $\omega_l(B_{1g})$ appeared in both of the diagonal scattering configurations $\bar{z}(xx)z$ and $\bar{z}(yy)z$; hence the two polarized modes could not be distinguished in practice. In the cubic phase $a^+a^+a^+$ with $T < T_L$ the vibrations $A_g(\alpha_{xx}+\alpha_{yy}+\alpha_{zz})$ and

$$E_g(\alpha_{xx}+\alpha_{yy}-2\alpha_{zz},\ \alpha_{xx}-\alpha_{yy})$$

have the Raman tensors

$$A_g:\ \begin{pmatrix} a & 0 & 0 \\ 0 & a & 0 \\ 0 & 0 & a \end{pmatrix};$$

$$E_g:\ \frac{1}{\sqrt{6}}\begin{pmatrix} b & 0 & 0 \\ 0 & b & 0 \\ 0 & 0 & -2b \end{pmatrix},\ \frac{1}{\sqrt{2}}\begin{pmatrix} b & 0 & 0 \\ 0 & -b & 0 \\ 0 & 0 & 0 \end{pmatrix}.$$

The laser polarization in these Raman experiments was always parallel to one of the (100) edges of the cubic crystals. Therefore, in agreement with the experimental observations for $T < T_L$, the results in Table III imply that the Raman lines $\omega_u(A_g)$ and $\omega_l(E_g)$ should be (i) polarized and (ii) indistinguishable from each other on the basis of polarization properties, in the geometry used for these measurements. Finally, in the one tilt phase $a^0a^0c^+$, the mode $\omega_u(A_{1g})$ is the single, completely symmetric soft mode observed in the Raman spectra for $T_M < T < T_U$ which could be observed only in the diagonal polarization configurations.

In Fig. 16, the eigenvector displacements for the $\vec{k}=0$ soft modes for the octahedral-tilt structures in Na_xWO_3 are indicated by arrows; in each phase the vibrational eigenvector $\vec{b}^{A_{1g}}$ corresponds also to the static displacements which comprise the rigid tilt lattice distortion. The soft-mode eigenvectors have been written out explicitly in Table IV. Note that the motion associated with one member of the E_g pair (for $a^+a^+a^+$) is given by

$$\mathrm{Re}\,\vec{b}^{E_g,1}(\vec{k}=0)e^{-i\omega t}=\vec{b}_3(\vec{k}_3)\cos\omega t + \vec{b}_1(\vec{k}_1)\cos\left(\omega t-\tfrac{2}{3}\pi\right) + \vec{b}_2(\vec{k}_2)\cos\left(\omega t-\tfrac{4}{3}\pi\right). \quad (21)$$

Accordingly, each oxygen atom orbits its equilibrium position in an ellipse with major to minor axis ratio

$$\frac{a}{b}=[(1-\cos\tfrac{2}{3}\pi)/(1+\cos\tfrac{2}{3}\pi)]^{1/2}=\sqrt{3}.$$

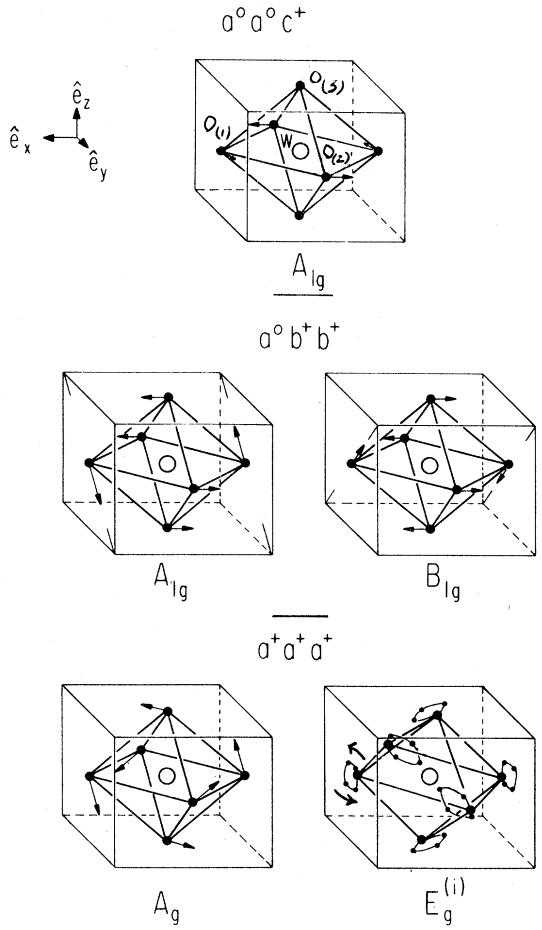

FIG. 16. Eigenvector displacements for the soft modes in Na_xWO_3.

All of the $\vec{k}=0$ vibrations of Na_xWO_3 were listed in Table II. It is interesting that the eigenvector displacements of each of the $\vec{k}=0$ optic normal modes—excluding the soft modes A_{1g} in $a^0a^0c^+$, $A_{1g}+B_{1g}$ in $a^0b^+b^+$, and $A_{1g}+E_g$ in $a^+a^+a^+$—will serve to *deform* the WO_6 octahedral units. As an example, the displacements for the Raman-active mode $\vec{b}^{B_{1g}}(\vec{k}=0)$ of the structure $a^0a^0c^+$ are indicated in Fig. 17. The resistance to distortion of the octahedral units in Na_xWO_3 not only constrains the possible displacive transitions accessible to the crystal starting from the high-temperature perovskite structure, but also results in an apparent reduction in the number of vibrational degrees of freedom of the lattice. In effect the rigidity of the WO_6 octahedra must separate the vibrational spectrum into high- and low-frequency bands which correspond, respectively, to W-O stretching modes which deform the octahedra, and the soft, external mode or rigid rotations of the WO_6 units. In addition, the soft vibrations might be expected to exhibit relatively large Raman scattering

TABLE IV. Eigenvector displacements of the soft modes. It suffices to specify the displacements of the oxygen atoms $O_{(1)}$, $O_{(2)}$, and $O_{(3)}$ in the perovskite primitive cell; the symbol $u_{i,\alpha}$ denotes a unit displacement of atom $O_{(i)}$ in the direction e_α, $\alpha = x,y,z$.

Na_xWO_3 soft-mode eigenvectors	
$a^0a^0a^0$	$\vec{b}^{A_{2g}}(\vec{k}=\frac{1}{2}\vec{K}_x+\frac{1}{2}\vec{K}_y) = u_{1,y}(a_p/2)\phi - u_{2,x}(b_p/2)\phi$
$a^0a^0c^+$	$\vec{b}^{A_{1g}}(\vec{k}=0) = u_{1,y}(a_p/2)\phi - u_{2,x}(b_p/2)\phi$
$a^0b^+b^+$	$\vec{b}^{A_{1g}}(\vec{k}=0) = (u_{1,y}-u_{1,z})(a_p/2)\phi - u_{2,x}(b_p/2)\phi + u_{3,x}(c_p/2)\phi$
	$\vec{b}^{B_{1g}}(\vec{k}=0) = (u_{1,y}+u_{1,z})(a_p/2)\phi - u_{2,x}(b_p/2)\phi - u_{3,x}(c_p/2)\phi$
$a^+a^+a^+$	$\vec{b}^{A_g}(\vec{k}=0) = (u_{1,y}-u_{1,z})(a_p/2)\phi + (u_{2,z}-u_{2,x})(b_p/2)\phi + (u_{3x}-u_{3,y})(c_p/2)\phi$
	$\mathrm{Re}[\vec{b}^{E_g,1}(\vec{k}=0)e^{i\omega t}] = [u_{1,y}\cos\omega t - u_{1,z}\cos(\omega t - 4\pi/3)](a_p/2)\phi + [u_{2,z}\cos(\omega t - 2\pi/3) - u_{2,x}\cos\omega t](b_p/2)\phi + [u_{3,x}\cos(\omega t - 4\pi/3) - u_{3,y}\cos(\omega t - 2\pi/3)](c_p/2)\phi$

cross sections compared to the "hard", internal vibrations at higher frequency, due to (i) the large soft-mode displacement amplitude[44]

$$\frac{\langle u_{\text{soft}}\rangle}{\langle u_{\text{hard}}\rangle} \approx \frac{\omega^2_{\text{hard}}}{\omega^2_{\text{soft}}} \sim 10^1 \text{ or } 10^2$$

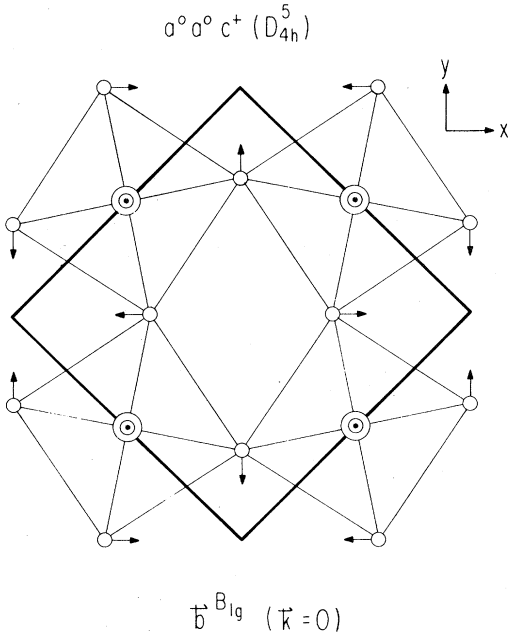

FIG. 17. Eigenvector displacements that deform the WO_6 octahedra in the phase $a^0a^0c^+$.

and (ii) the relaxed bonding configuration associated with the soft-mode displacements. It was emphasized earlier that no Raman bands were resolved from the background continuum scattering outside the low-frequency region $0 < \omega < 150$ cm^{-1} in the Raman spectra reported here. However, the vibrations of pure single crystal WO_3 shown in Fig. 18 are clearly grouped into high- and low-frequency regions, representing the internal and external modes of the rigid WO_6 units, while comparable scattering efficiencies are exhibited by the internal and external vibrations. Evidently the inferred reduced scattering efficiencies for the WO_6 internal vibrations in Na_xWO_3 is intimately related to the presence of the conduction electrons and to the topological disorder. While the

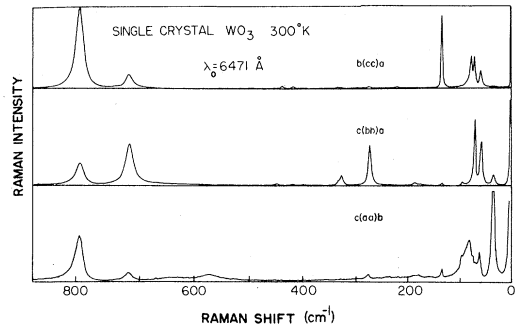

FIG. 18. Raman spectra of single crystal WO_3. The monoclinic axis is denoted by b. These spectra were recorded with 10-mW krypton laser radiation at $\lambda_0 = 6471$ Å.

rigid tilts involve no motion of the Na^+ ions, the internal modes may be strongly coupled to the Na^+ degrees of freedom, resulting in the dissipation of the vibrational energy, the loss of long-range coherence of the phonons, and over-all broadening and reduced intensity of the Raman bands.

A qualitative picture of the phase transitions in Na_xWO_3 is the following. If a uniform decrease in the W-W distances occurs, as by lowering the temperature, the rigid WO_6 octahedra will accommodate the lattice distortion by the correlated rigid tilts which minimize the deformation of the WO_6 units. As the lattice contracts the order parameter (i.e., the tilt angle) and therefore the soft-mode frequencies must increase. This behavior is clearly exhibited by $\omega_u(T)$ and $\omega_l(T)$ in Fig. 9; however, when the contraction of the lattice reaches its low-temperature limit, $\omega_u(T)$ and $\omega_l(T)$ become *independent* of temperature. Therefore each sodium-tungsten bronze sample can be characterized by the constant, low-temperature value of $\omega_u(10 < T < 50\ \text{K})$, to be denoted by $\omega_c(x)$. Figure 19 shows the linear dependence of ω_c^2 on x for $0.6 < x < 1$. Noting that $\omega_c^2(x=0.52)$ deviates from the straight line, we recall from Sec. II the fact that the purple sodium-tungsten bronzes $0.5 < x < 0.6$ differ from crystals in the concentration range $0.6 < x < 1$ in their growth habit and in the difficulty with which they are cleaved. In fact, the sample $Na_{x=0.52}WO_3$ possesses a cubic structure at all temperatures,[29] although no octahedral tilt structure has been assigned. At $T=10$ K the purple bronze exhibits two Raman bands which are not present at room temperature; possibly, the second-order transition $a^+a^+a^+ \rightarrow a^0a^0a^0$ occurs at 300 K or below.

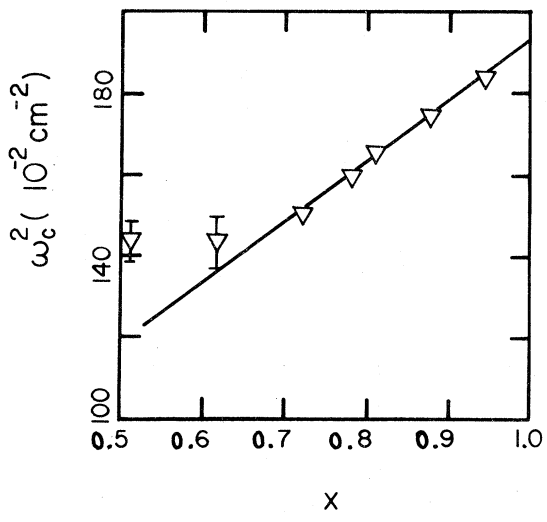

FIG. 19. Plot of the temperature-independent low-temperature value of $\omega_u(T)$ vs x.

V. CONCLUSION

The Raman scattering data presented here have been shown to be consistent with the rigid tilt space-group assignments for the four distinct structural phases of Na_xWO_3 with $0.6 < x < 1$ inasmuch as the observed Raman bands and their polarization properties can be accounted for among the $\vec{k}=0$ Raman-active lattice vibrations of the rigid tilt structures $a^0a^0a^0$, $a^0a^0c^+$, $a^0b^+b^+$, and $a^+a^+a^+$ proposed by Clarke. But the assumption that the WO_6 octahedral units in Na_xWO_3 remain regular regardless of the structural phase transitions, an assumption that is central to the interpretaion of the x-ray data of Clarke, has been correlated with experimental evidence for the rigidity of the octahedral units provided by the light scattering studies reported here. In fact, the resistance to distortion of the corner-linked octahedra in Na_xWO_3 is a fundamental physical characteristic that governs the thermodynamic, structural, and lattice-dynamical properties of these materials. While the phase transition temperatures $T_U(x)$, $T_M(x)$, and $T_L(x)$ could be determined both from the Raman data and from x-ray data, the mutually complementary structural and dynamical information have provided for the first time an elucidation of the structural phases that occur in Na_xWO_3. Although rigid tilt structures are frequently encountered among ceramic perovskites, the successive "positive" tilts exhibited by the metallic crystals Na_xWO_3 are unique. In the context of the Landau theory, the rigid tilt structures of Na_xWO_3 are derived from the ideal perovskite structure by one of the simplest possible sequences of structural phase transitions that involves the participation of a multicomponent order parameter[25] belonging to a single irreducible representation of the space group O_h^1. Furthermore, the vector order parameter $\{c_1,c_2,c_3\}$ subduces one or more irreducible representations of the corresponding rigid tilt space group at $\vec{k}=0$. These irreducible representations coincide with the symmetries of the observed Raman-active soft modes in Na_xWO_3, whose eigenvectors are linear combinations of the "positive" tilt lattice distortions.

It should be noted that the high-temperature second-order phase transition in Na_xWO_3, involves a doubling of the primitive cell, and the space group D_{4h}^5 of the resulting structure is *not polar*. Therefore the designation "ferroelectric metal" is inappropriate for Na_xWO_3. However, as pointed out by Clarke,[17] the successive re-orientation of the vector order parameter as the temperature is decreased, $\{0,0,0\}$, $\{0,0,c_3\}$, $\{0,c_2,c_3\}$, $\{c_1,c_2,c_3\}$ constitutes a structural analogy to the sequence of ferroelectric transitions in $BaTiO_3$ in which the vector order parameter—i.e., the polarization—is directed alternately along the axes (0,0,1), (0,1,1), and (1,1,1) of the pseudocubic cell.

As discussed earlier with reference to the phase di-

agram for Na_xWO_3 in Fig. 3, the upper and lower phase transitions which occur at the temperatures $T_U(x)$ and $T_L(x)$, had been detected also in reflectivity, specific heat and NQR measurements. However the tetragonal-tetragonal ($a^0b^+b^+$-$a^0a^0c^+$) phase boundary at $T = T_M(x)$ was observed apparently only in the x-ray and light scattering experiments. In retrospect, the existence of the tetragonal-tetragonal phase boundary might have been anticipated, in view of the reflectivity and NQR results, inasmuch as the twinning of tetragonal domains in Na_xWO_3 along (110) planes at temperatures $T > T_L$, as observed in polarized reflectance from Na_xWO_3 single-crystals surfaces, cannot be reconciled with the rigid tilt structure $a^0a^0c^+$ proposed by Borsa in order to account for the NQR data at temperatures $T < T_U$. Furthermore it is surprising that the phase transition at $T = T_M(x)$ was not observed in both the reflectance and the NQR experiments. Not only does the first-order tetragonal-tetragonal transition $a^0b^+b^+$-$a^0a^0c^+$ entail a change in the domain structure of the Na_xWO_3 crystal, but a discontinuous change in the quadrupole coupling constant for Na^{23} can be expected at the first-order transition temperatures $T = T_L(x)$ and $T = T_M(x)$, due to the rearrangement of the 12 sodium nearest neighbors, associated with the structural transitions, and due to the changing contribution to the rms electric field at the Na^{23} site that is attributable to the soft-mode fluctuations. In addition to the NQR and reflectance experiments, the results of optical, neutron, and transport measurements carried out prior to the Raman and x-ray work discussed here warrant reexamination in view of the present understanding of the structure and phase transitions in Na_xWO_3.

An extension of the present work must, first of all, address the polarization properties of the Raman-active soft modes in "cubic" Na_xWO_3, especially in the two-tilt tetragonal phase $a^0b^+b^+$ where the A_{1g} and B_{1g} modes should be unambiguously identifiable from their polarization characteristics, provided a sufficiently large tetragonal single domain can be prepared and properly oriented. A large single domain might be obtained by applying mechanical stress to the samples, while the orientation of the domains can be simultaneously observed in polarized reflectance. In addition, the application of stress or hydrostatic pressure to crystals of Na_xWO_3 would extend the phase diagram in Fig. 3, possibly resulting in the observation of new rigid tilt structures in Na_xWO_3, or a rearrangement of the structural sequence exhibited in the absence of externally applied pressure or stress. Future light scattering studies of the sodium-tungsten bronzes at lower concentrations $0 < x < 0.5$ will be motiviated by the interesting electronic properties, such as superconductivity and the metal-nonmetal transition at $x = 0.2$, and the possibility of structural transitions in the tetragonal I and tetragonal II phases. In light scattering studies of other alkali tungsten bronzes, as well as the amorphous electrochromic tungsten oxide and tungsten bronze thin films, a host of interrelated physical and structural properties that are intrinsically interesting and also of possible technological significance will, no doubt, be encountered.

ACKNOWLEDGMENTS

The author wishes especially to thank Professor S. A. Solin for suggesting this project and for his support and useful suggestions during its completion. Also, helpful discussions with R. Clarke, P. Horn, and R. J. Nemanich are acknowledged. This research was supported in part by the DOE. It has also benefitted from the support of the University of Chicago Materials Preparation Laboratory by the NSF.

---

*Submitted in partial fulfillment of the requirements for the Ph.D. degree at the University of Chicago. Present address: Bell Laboratories, Murray Hill, N.J. 07974.

[1]P. G. Dickens and M. S. Whittingham, Quart. Rev. Chem. Soc. 22, 30 (1968).
[2]M. J. Sienko, Adv. Chem. 39, 224 (1963).
[3]H. R. Shanks, J. Crystal Growth 13/14, 433 (1972).
[4]M. Atoji and R. E. Rundle, J. Chem. Phys. 32, 627 (1959).
[5]S. Fujeida, Sci. Light (Tokyo) 18, 1 (1969).
[6]D. W. Lynch, R. Rosei, J. H. Weaver, and C. G. Olsen, J. Solid State Chem. 8, 242 (1973).
[7]J. H. Ingold and R. C. DeVries, Acta Metal. 6, 736 (1958).
[8]J. F. Scott, R. F. Leheny, J. P. Remeika, and A. R. Sweedler, Phys. Rev. B 2, 3883 (1970).
[9]E. Salje, Ferroelectrics 12, 215 (1976).
[10]H. Inaba and K. Naito, J. Solid State Chem. 15, 283 (1975).
[11]H. R. Shanks and R. D. Redin, J. Chem. Phys. Solids 27, 75 (1966).
[12]H. R. Shanks, P. H. Sidles, and G. C. Danielson, Adv. Chem. 39, 237 (1963).
[13]G. Hägg and A. Magneli, Rev. Pure Appl. Chem. (Australia) 4, 235 (1954).
[14]G. Bonera, F. Borsa, M. L. Crippa, and A. Rigamonti, Phys. Rev. B 4, 52 (1971).
[15]A. T. Fromhold and A. Narath, Phys. Rev. 136, 487 (1964).
[16]E. J. Flynn, S. A. Solin, and H. R. Shanks, Solid State Commun. 25, 743 (1978).
[17]R. Clarke, Phys. Rev. Lett. 39, 1550 (1977).
[18]A. M. Glazer, Acta Crystallogr. Sect. B 28, 3384 (1972).
[19]J. F. Scott, Rev. Mod. Phys. 46, 83 (1974).

[20]P. W. Anderson and E. I. Blount, Phys. Rev. Lett. 14, 217 (1965).
[21]W. Cochran, Adv. Phys. 9, 387 (1960).
[22]E. J. Flynn, S. A. Solin, and H. R. Shanks, Bull. Am. Phys. Soc. 22, 260 (1970).
[23]F. Borsa, *Proceedings of the International School of Physics 'Enrico Fermi,'* Course LIX (North-Holland, Amsterdam, 1976), p. 255.
[24]L. D. Landau and E. M. Lifshitz, *Statistical Physics* (Pergamon, Oxford, 1958).
[25]E. B. Vinberg, Yu. M. Gufan, V. P. Sahknenko, and Yu. I. Sorotin, Sov. Phys. Cryst. 19, 10 (1969).
[26]K. S. Aleksandrov, Sov. Phys. Cryst. 21, 133 (1976).
[27]A. G. Khachaturyan, Sov. Phys. Dokl. 10, 1212 (1966).
[28]C. Haas, Phys. Rev. 140, 863 (1965).
[29]R. Clarke (private communication).
[30]D. M. Hwang and S. A. Solin, Appl. Phys. Lett. 20, 181 (1972).
[31]T. C. Damen, S. P. S. Porto, and B. Tell, Phys. Rev. 142, 570 (1966).
[32]G. E. Devlin, J. L. Davis, L. Chase, and S. Geschwind, Appl. Phys. Lett. 19, 138 (1971).
[33]A. A. Maradudin and S. H. Vosko, Rev. Mod. Phys. 40, 1 (1968).
[34]M. Lax, *Symmetry Principles in Solid State and Molecular Physics* (Wiley, New York, 1974).
[35]V. Heine, *Group Theory and Quantum Mechanics* (Pergamon, Oxford, 1960).
[36]R. Loudon, Adv. Phys. 13, 465 (1964).
[37]R. Shuker and R. W. Gammon, Phys. Rev. Lett. 25, 222 (1970).
[38]R. J. Nemanich and S. A. Solin, Bull. Am. Phys. Soc. 20, 429 (1975).
[39]M. V. Klein, J. A. Holy, and W. S. Williams, Phys. Rev. B 17, 1546 (1978).
[40]H. R. Shanks (unpublished).
[41]H. Winston and R. S. Halford, J. Chem. Phys. 17, 607 (1949).
[42]*International Tables for X-ray Crystallography*, edited by J. S. Kasper and K. Lonsdale (Kynoch, Birmingham, England, 1972), Vol. 1.
[43]J. L. Birman, Phys. Rev. Lett. 17, 1216 (1966).
[44]P. C. Kwok and P. B. Miller, Phys. Rev. 151, 387 (1966).